Peer-to-Peer Networking and Applications (2021) 14:3181–3197
https://doi.org/10.1007/s12083-021-01101-w

Path loss modelling at 60 GHz mmWave based on cognitive 3D ray tracing algorithm in 5G

Usman Rauf Kamboh[1] · Ubaid Ullah[1] · Shehzad Khalid[2] · Umar Raza[3] · Chinmay Chakraborty[4] · Fadi Al-Turjman[5]

Received: 17 November 2020 / Accepted: 10 February 2021 / Published online: 11 March 2021

Abstract
The objective of the study is to consider the foremost high-tech issue of mobile radio propagation i.e. path loss for an outdoor and indoor environment for mmWave in a densely populated area.60 [GHz] mmWave is a win-win for the 5th Generation radio network. Several measurements and simulations are performed using the simulator "Smart Cognitive 3D Ray Tracer" build in MATLAB. Two of the main parameters (pathloss and received signal strength (RSS)) of the radio propagation are obtained in this study. To compute the pathloss and RSS, 5G 3GPP mobile propagation model is selected due to its flexibility of scenario and conditions beyond 6 GHz frequency. For indoor simulations, we again chose 5G 3GPP mobile propagation model. It is evident from the recent previous studies that there is still not enough findings in the ray tracing specially cognitive 3D ray tracing. The suggested alternative cognitive algorithm here deals with less iterations and effective use of resources. The conclusions of this work also comprise that the path loss is reliant on separation distance of base station and receiver. The above mentioned frequency and interconnected distance reported here provide better knowledge of mobile radio channel attributes and can be also used to design and estimate the performance of the future generation (5G) mobile networks.

Keywords Path loss · 60 [GHz] · 5G · mmWave · Cognitive radio networks · RF · 3D ray tracing algorithm · RSSI

1 Introduction

The growth of telecommunication sector and the increasing number of smart phones have forced cellular network providers to serve higher data rates than previously served data rates. That's why the Mobile Network Operators need a techno-economic approach to deal with the demand for increasing data rates. Therefore, an algorithm is necessary to be developed to cope up with the delay, path loss and received signal strength. [1] The mobile radio channel places fundamental limits on the efficiency of wireless communication systems.The major distinctive characteristic in which 5G wireless differs from the traditional wireless systems is that 5G allocates high bandwidth in unit area, possibly by exploiting Cognitive Radio, for enabling large number of connected devices for longer duration. [35] The radio path between generator and analyser can severely obstructed by vertical buildings, foothills,vehicles and vegetation expect direct path. Modeling the path loss (PL) has one of the most problematic phase as compared to the wired one, which is normally design on observed measurements.

Figure 1 demonstrates the 2D view of two ray ground reflection model for the concerned scenario. The ray indicated in color blue collides with the ground bends by the angle θ before reaching to mobile station (MS). Same is the case for far-wall and random ray. The large-scale PL typically studied in 3GPP release 17 for outdoor and indoor environment. After the free space propagation model, a number of well-known outdoor propagation models have been used to predict PL over irregular terrain like Longley-Rice, Durkin's, Okumura-Hata and the extension of hata COST-231. For In-building, the Log-distance and Ericsson Breakpoint models are common with attenuation factor and signal penetration loss. All aforementioned models have been used to predict the signal strength over measurements and transmitter–receiver (Tx-Rx) separation in the specific

This article belongs of the Topical Collection: *Special Issue on Cognitive Models for Peer-to-Peer Networking in 5G and Beyond Networks and Systems*
Guest Editors: Anil Kumar Budati, George Ghinea, Dileep Kumar Yadav and R. Hafeez Basha

✉ Usman Rauf Kamboh
usman.rauf@tuf.edu.pk

Extended author information available on the last page of the article.

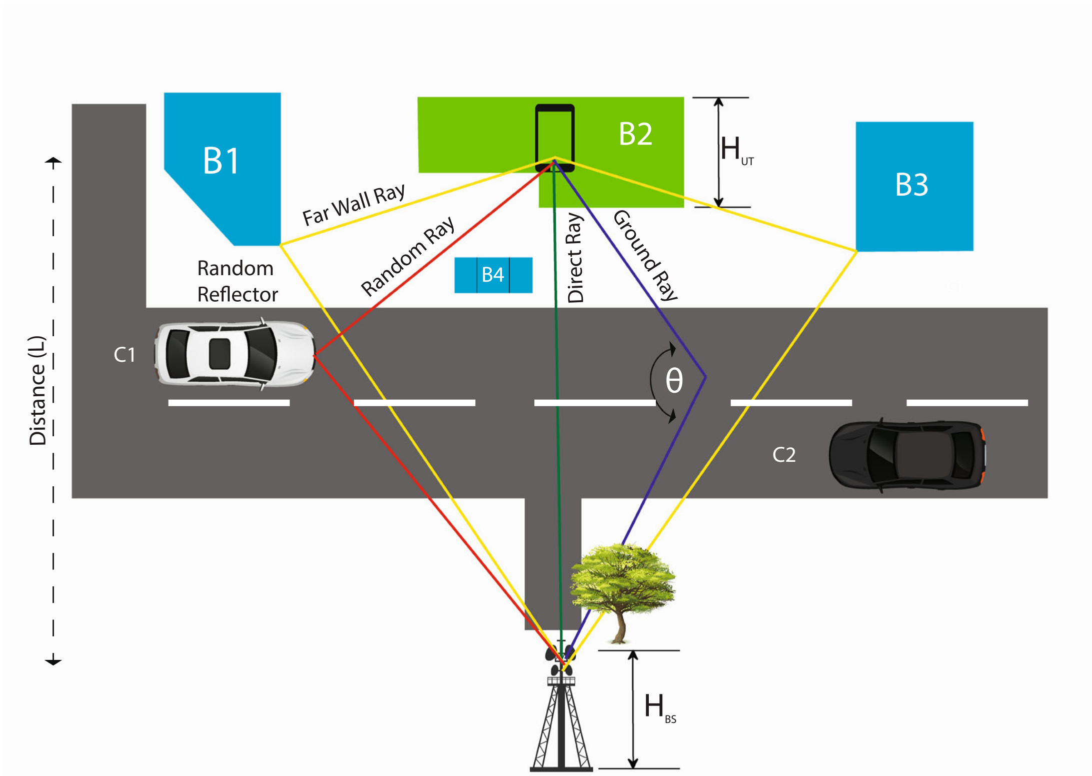

Fig. 1 Mobile Radio Path Distribution

scenario [2] - [3]. Well, each model is resulting with different characteristics, in [2], the measurement were carry out 0.9 [GHz] and 1.8 [GHz] for Outdoor to Indoor (O2I) environment based on COST-231 model. However, Millimeter-wave (mmWave) identified as primary fuel for the fifth generation (5G) mobile communication system. The band range about 30 [GHz] to 300 [GHz] have number of unregistered radio channels and can deliver [GHz] level bands of contiguous ranges, and therefore becoming a significant entrant in provision the high-throughput wireless connection for future mobile standard. As compared the high operating frequencies with traditional ranges under 6 [GHz], the attenuation factor experienced high on each metre due to the small-wavelengths and as well atmosphere [4] - [5]. As a result of the above mentioned problem, 5G networks have to work on latest trends. On the other hand due to the cognition handling in the mmWave networks, this is becoming very complicated and complex. [18] In-building, 60 [GHz] spectrum has been proposed to offer determined throughput for direct and indirect path. So far, a number of studies have been directed to measure the signal strength and attenuation of materials at higher frequency band for cognitive radio networks. Following the both Line-of-Sight (LoS) and None-Line-of-Sight(NLoS) environments, the intensive measurements campaigns for the perception of PL of several obstacles at 28 [GHz], 38 [GHz], 60 [GHZ] and 73 [GHz] In-building workplace environment were studied in [6] - [10].

As above mentioned studies, there is still a large slot to inquire the dimensions of mmWave to achieve the ultimate objective as follows. The most recent works are emphasized on 28 [GHz] and the 38 [GHz] frequency bands considering as primary vehicle, however there are still other possible bands up to 300 [GHz] that can be further discovered. (See Table 1)

For purpose of demonstration, the method of images (ray-tracing) have been designed in Fig 1. The geometry presented in Fig. 1 illustrate the path difference between direct ray, ground ray, random ray and far wall ray effectively; although, for establishing the applied models in radio propagation based on ray-tracing, several years have gone into the study and exploration to make estimations that can give back the specific environment [1]. The method of ray-tracing for radio channel was derived from image-theory. Geometric optics and uniform theory of refraction were used to analyse that all transmitted rays reached by

Table 1 Recent Studies Related to Propagation

Reference	Max. rays	mmWave Frequency	Max Distance	Reported Parameters
[20]	2	6 GHz	10,000m	PL, Pr
[21]	20	1 GHz, 1.8 GHz, 2.4 GHz	10,000m	PL, PLE
[22]	2	1500 MHz	1000m	PLE
[23]	3	3600 MHz, 10. 6 GHz	0.1 km	PL
[24]	3	1.9 GHz	0.4 km	Propagation
[25]	62	60 GHz to 1000GHz	0.006 km	Channel Capacity, Distance, Frequency
[26]	9	60 GHz	0.06 km LoS and 0.025 km nLoS	Pr
[27]	5	2.4 GHz	0.05 km	Pr
[28]	Multiple rays	94 GHz	0.006 km	PL, propagation path analysis
[29]	4	94 GHz	0.0015 km	Pr for radars
[30]	10	2.4 GHz	0.001 km	PL, Pr
[31]	11	28 GHz	0.04 km indoor and 0.1 km outdoor	Pr, PL, Gr, Gt
[1]	Multiple Rays	28 GHz	110 m indoor and 45 m outdoor	PL, Pr
This Paper	Multiple Rays	60 GHz	110 m indoor and 50	PL, Pr, RSSI

the receiver. Basically, the ray-tracing methods are used to model electromagnetic environment by projecting the propagating paths between source and destination. In the method of images, the shooting and bouncing ray approach is the key driver for the paths estimation [11] - [12]. To make computational algorithm less complex and to decrease the amout of memory used, walls of the building are illustrated as smooth surfaces and flat slabs. This simplification forces the reflected and diffracted rays to be tackled using "image-RT approach" and to the Uniform Theory of Diffraction (UTD) [20] (Table 2).

Figure 2 indicates the recent related work. The author [1] predicted path loss as well as received signal strength in outdoor and indoor environment respectively. Following the above image theory, the Ray Tracing (RT) based algorithm was designed by Ikegami et al [13]. The earlier well-known RT methods, brute force RT [14] and image theory [15] faced some limitations. The brute force check all possible paths using regular angular sampling method, however due to the increasing angular separation and dropping angles could result in the loss of some paths. On the other side, the image theory technique is not fit for complex environments, since its point to point ray targeting and unreliability of radiated rays. The proposed method can calculate the losses in densely populated area for both outdoor and indoor environment.

The rest of this article is structured as follows. The In-building offices environment (in which measurement set-up is installed) is discussed in Section 2. The Path Loss (PL) mathematical modeling is inquired in Section 3. The smart 3D ray tracing algorithm for the under consideration scenario is explain in Section 5. The analysis of obtained results is discussed in Section 6. Finally, we draw a conclusion and future work in Section 7.

2 Measurement environment

The measurement set-up comprising on urban macro cell (UMa) mounted with small base stations has been considered. Both devices are assumed to be working on same radio frequencies (60 [GHz]) under subscriber group (CSG). Considering the capacity coverage, throughput and traffic offload, we deployed the small base station MetroLinq (ML). In our scenario, all Tx were on fixed location and users (Rx) were moving in indoor. The propagation measurements at 60 [GHz] were inquired in summer of 2020 at outdoor and indoor environment located at the State Life Building of Lyallpur, Pakistan.

The satellite view of the concerned scenario for urban area is shown in Fig. 3. The four high-rise buildings B1, B2, B3 & B4 were investigated in proposed scenario for pathloss and angular power, where elevation of main experimental building B2 is 50.4 [m]. B2 comprises of 13 office floors. The parking area and basement are not included during measurement campaign. There are two random reflector cars (C1 and C2) in main street in red and white color, also marked in the photograph in Fig. 3. The transmitter tinted with blue ring is set at a height of 25 [m] with a 110 [m] Tx-Rx maximum separation. The distance from UMa to User Interface (UIs) fluctuate as the user change their location from O2I or indoor to indoor (I2I). The material used in building also varies as the outer walls of B1 and B3 are fabricated with infrared coated glass and B4 outer-inner mostly made-up with cemented and plywood structure.

For I2I scenario, Fig. 4a shows the locations of Tx mounted on the walls of the corridor. The height of the Tx as indicated in the fig is 2.7 [m]. Figure 4b indicates the set-up and receiving equipment. The users on the floor are distributed in such a fashion that there are 8 to 16 mobile

Table 2 Ray Tracing Techniques Comparison

Parameters / Model	Shooting and Bouncing [32]	Brute Force [33]	Genetic Algorithm [34]	Our Proposed Model
Angles	0° to +360°	-90° to +90°	0° to +90°	-360° to +360°
Trajectory	Straight	Reflected and Diffracted	Reflected and Diffracted	Reflected, Diffracted, Deflected and refracted
Symmetry of infrastructure	Symmetrical	Symmetrical	Unsymmetrical	Unsymmetrical
Frequency Range	900MHz	900MHz	150 Hz -1.5 GHz	0-50Ghz
Distance	0.577 km	0.577km	0-20km	0 – 150km
Path	LOS	LOS	LOS/NLOS	LOS/NLOS
Environment	O2O	Site-Specific	I2I, O2I	I2O, O2I, O2O, I2I
Computational Time	180 mins	N/A	150 mins	130 mins

users on each floor all the time. At each position, the Tx is piloted to the direction of the office while the Rx was set aside in the horizontal height and moved in azimuth-domain from 0° to 360° with continual increments. To considering the measurement, the Tx-Rx maximum altitude are aligned 2500-5040 cm respectively. The rest of parameters and measurements are in Table 3.

Figure 5 is the complete floor plan of the under consideration building. There are three Acess Points (APs) i.e. Tx1, Tx2 and Tx3 marked with green circles, mounted on the wall and the receiver illustrated with red circle is inside the concerned room. Considering the above measurement setup, our research gear is to compute the PL on 60 [GHz] mmWave using cognitive 3D RT algorithm, which will examine the performance of UMa and ML in outdoor and indoor environment respectively. The measurement objective is to check the behaviour of algorithm over losses due to in-between obstacles and also to compute the received signal strength of remote users within the building.

3 Path loss modelling

The PL is the inverse of the instantaneous local channel gain [16]. Electromagnetic waves are well known for the attributes like reflection, diffraction and scattering. The loss estimation comprises on building structure as well as its electromagnetic wave interaction with different objects. The substances includes the reflection constants, permittivity, conductivity, roughness and polarization information.

3.1 Path loss modeling for urban-macro O2I

The total path loss for Line-of-Sight (LoS) and None-Line-of-Sight (NLoS) is modeled here as [2]:

$$L_{P_{TOT}} = L_{P_{TYP}} + L_{P_{TB}} + L_{P_{IB}} + Z(0, \sigma_P^2) + Z(0, \sigma_{SF}^2) + \mu \quad (1)$$

where $L_{P_{TYP}}$ is the typical path loss, $L_{P_{TB}}$ is the through building dispersion losses from concrete outer-wall and $L_{P_{IB}}$ is the in-Building loss where radio signal penetrate in different materials. The standard deviation for the dispersion losses is derived as σ_P^2 and σ_{SF}^2 is the average deviation for the shadow fading. μ is used for vehicle penetration loss and O2I vehicle penetration loss models are correct for upto 0.6-60 [GHz].

$$L_{P_{TYP}} = L_{P_{UMa}}(S_{3D_{out}} + S_{3D_{in}}) \quad (2)$$

where $L_{P_{UMa}}$ is the urban macro path loss, $S_{3D_{out}}$ is the three dimensional outdoor distance from the tip of T_x to the outer wall of the building and $S_{3D_{in}}$ is the inside three dimensional

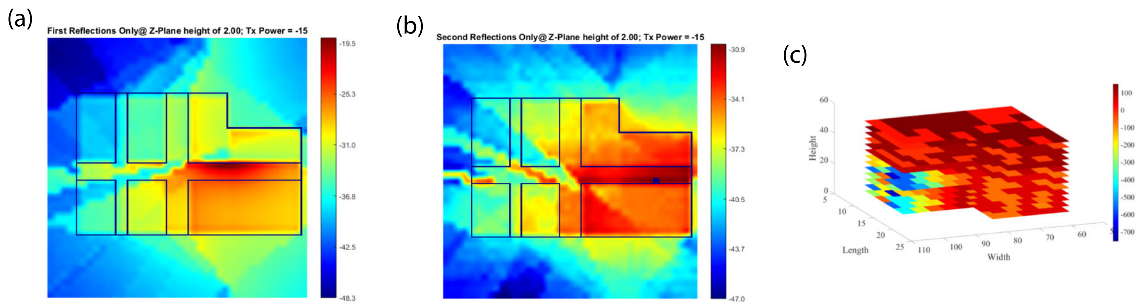

Fig. 2 Recent related work

distance. In Fig. 6 it can be seen that 3D distance can be computed by adding both indoor and outdoor distances as well as the height of the H_{UI}. Figure 6 describe the floor-wise descriptions of parameters, either it is LoS or NLoS and also guide about path as received through ground or through wall.

Figure 7a indicates the empirical CDF which suddenly irrupts at about 80 [m] which is clearly a sign of concern for modelling the algorithm. Figure 7b shows the outage probability of BS for different frequencies.

$$L_{P_{UMa-LoS}} = \begin{cases} L_{P_1} & 10[m] \leqslant S_{2D} \leqslant S'_{BP} \\ L_{P_2} & S'_{BP} \leqslant S_{2D} \leqslant 5[m] \end{cases} \quad (3)$$

where $L_{P_{UMa-LoS}}$ indicates the function used for the propagation loss in urban-macro scenario, in LoS case if the $T_x - R_x$ distance $\leq$ breakpoint and which is given as,

$$S_{BP'} = 13.33 h'_{BS} h'_{UI} f_c \quad (4)$$

where f_c is the high operating frequency in [Hz], and h'_{BS} and h'_{UI} are the effective antenna altitudes of base station and user interface. To compute h'_{BS} and h'_{UI} we need to subtract the environment influence $h_E = 1$ from respective antenna heights. So far according to base station and user interface brake-point distance, we follow the L_{P_2} in our measurement from given equations:

$$L_{P_1} = 32.2 + 40 * log_{10}(S_{3D}) + 20 * log_{10}(f_c) \quad (5)$$

$$L_{P_2} = 32.2 + 40 * log_{10}(S_{3D}) + 20 * log_{10}(f_c) - 10 * log_{10}((S_{BP'})^2 + (h_{BS} - h_{UI})^2) \quad (6)$$

To follow the urban-macro, the shadow fading factor for LoS is 4 [dB] and for NLoS is 6 [dB] when associated with a height 25 [m] or above. However in case of NLoS, we follow the max condition (b) for 10 [m] $\leq S_{BP'} \leq 5[Km]$ which apply as:

$$L_{P'_{UMa-NLoS}} = 13.54 + 39.08 * log_{10}(S_{3D}) + 20 * log_{10}(f_c) - 0.6 * (h_{UI} - 1.5) \quad (7)$$

In (3), (5), (6) and (7) S_{3D} is the total of outdoor and indoor distance or $S_{3D_{out}} + S_{3D_{in}}$, which is defined as:

$$S_{3D_{out}} + S_{3D_{in}} = S_{3D} = \sqrt{(S_{2D_{out}} + S_{2D_{in}})^2 + (h_{BS} - h_{UI})^2} \quad (8)$$

here, S_{2D} is two dimensional distance in-between base station and user interface of the building. It can also be denoted as $S_{2D_{out}} + S_{2D_{in}}$. Furthermore, the material permeation loss over frequencies demonstrated with the help of Table 2 are modelled here as [8]

$$L_{P_{TW}} = L_{P_{ad}} - 10 log_{10} \sum_{i=1}^{N} F_i 10^{\frac{L_{substance_{-i}}}{-10}} \quad (9)$$

$L_{P_{TW}}$ is an additional propagation loss which is to be studied through the outer-wall-loss over frequencies, $L_{substance_{-i}}$ is refer as the permeation loss, F_i is fraction of the i_{th} substances and N is the number of substances involved in wall penetration loss. The concerned building is constructed with multiple substances. Our simulator is not only modelled for traditional low-loss concrete structure but also for the high loss metal coated-glass for B1 and B2 individually shown in Table 2.

In Table 2, L_{SG} is the low path loss through standard glass, L_{Con} is the loss through concrete and L_{MCG} is the high loss through metal coated glass. Moreover, the

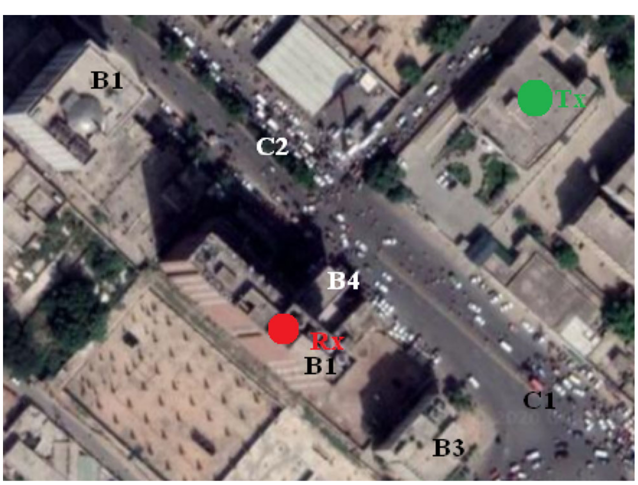

Fig. 3 Measurement Environment

(a) (b)

Fig. 4 Experimental Arrangements

use of such high loss glass at this time seems to be more predominant in organizational towers than in home construction in some countries of the world. The indoor loss of the building is given by [2]

$$L_{P_{IB}} = \sum_{i=1}^{M} \gamma S_{2D_{IN}} \tag{10}$$

In (10), γ is the material dependent constant as used inside the building. The value of γ vary for low, moderate and high penetration loss due to material M.

3.2 Path loss modelling I2I

The base stations operating on higher frequencies are much smaller in size and have greater throughput. The 60 [GHz] based small base station (SBS) therefore will not overcrowd poles, rooftops and corridors. Furthermore, a huge amount of noise-free-spectrum (6 – 12 [GHz]) makes the 60 [GHz] band perfect for high gain point-to-point and point to multipoint uses. The 60 [GHz] mmWave is categorized as very sensitive to oxygen-absorption which means signals spread from a 60 [GHz] mmWave will not travel as far as lower frequencies. Frequency reuse factor makes it perfect not only for countryside, but also for densely populated deployments [7]. Moreover, co-location of several components on a single tower is possible due to narrow-beam widths which are attained from both high-gain directional antennas as well as dedicated beamforming method. These benefits illustrate that 60 [GHz] avoid the cell-interference problems usually contained by other frequencies [7]. Measurements were performed after office hours for smooth readings. There are rooms and workshops, the doors were shut throughout the measurement along both side of its central corridor. A wall mounted Tx "ML" considered here in office building corridor operating at 60 [GHz] frequency and shown in Fig. 4a. The B1 first floor (open office) in the mentioned area is composed of concrete, plywood, coated glass and other materials. The thickness of the concrete walls that separate the main office from corridor on both sides is within the range of 24-65 [cm]. The indoor corridor Tx height is 2.7 [m] and is separated with Rx distance 6 [m] inside the office. For indoor path loss, we selected the 3GPP loss models with supportive range (6 [GHz] to 100 [GHz]) for LoS and NLoS to get the accurate results [9]. With the increasing width of the corridor and increasing the frequency, COST-231 model provides simulation results which are not considerable when compared to measurements. In [19], the author addressed the same issue. Considering the above factors, we have chosen 5G-3GPP model for our work. Figure 8 represent that, for inside first floor we need to mount three Tx in corridor to cover the traffic. In 3GPP open office scenario states that: [2]

$$L_{P_{ofc-LoS}} = 32.4 + 17.3 log_{10}(S_{3D}) + 20 log_{10}(f_c) \qquad 1[m] \le S_{3D} \le 100[m]$$

Table 3 Simulation Setup

Parameter	Description	Unit Value
Operating Frequency	mmWave	60 [GHz]
Scenario	Layout	LoS / NLoS
Number of Floors	13	
Cell Layout	Hexagonal grid	1 Macro Site
Wall	Height	2.7 [m]
	Thickness	0.1 [m]
Base Station	Transmit Power	20.1 [dBm]
	Height	24.5 [m]
	Antenna pattern	Omni 5 [Bi]
	Bandwith	0.1 [GHz]
	Reflection, Diffraction	Enabled
	Polarization	Vertical
User Terminal	Receiver Loss	2 [dBm]
	Height	2.7 [m]
	Antenna Pattern	Omni 5 [Bi]
	Bandwidth	0.1 [GHz]

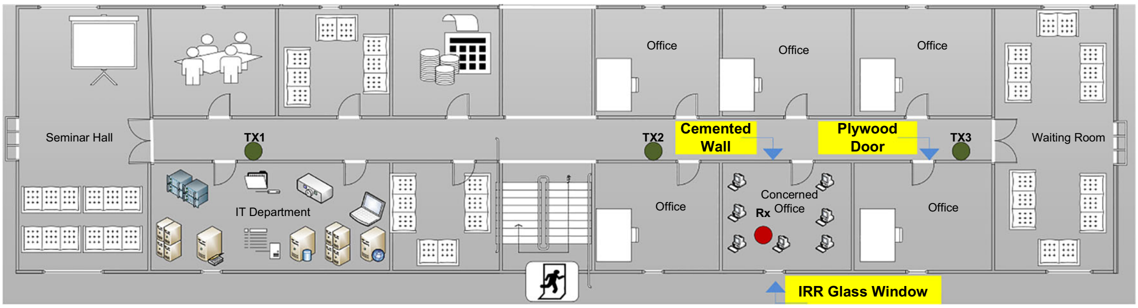

Fig. 5 T_x and R_x indoor locations

(11)

$$L_{P_{ofc-NLoS}} = max(L_{P_{ofc-LoS}}, L_{P_{ofc-NLoS}}) \tag{12}$$

$$L_{P_{ofc-NLoS}} = 38.3log_{10}(S_{3D}) + 17.20 + 24.9log_{10}(f_c) \quad 1[m] \leq S_{3D} \leq 86[m] \tag{13}$$

In (11) and (13), open office path loss LoS and $NLoS$ is the sum of free space PL and path loss exponent (PLE), where denotes the referred frequency of base station. S_{3D} is the three dimension distance between user interface and base station. Beside the open office scenario, 3GPP path loss models can be inquired in variety of places including shopping malls, street canyon, urban and rural areas. The omnidirectional PL models frequency supportive is in-between 0.5 [GHz] to 100 [GHz]. It is challenging to find the accurate received power level during complex indoor office scenario on higher operating frequencies. The Friis's equation is the simplest technique in radio propagation to compute the received power level in free space as used below

$$\frac{P_t}{P_r} = G_t.G_r(\frac{\lambda}{4\pi r})^2 \tag{14}$$

where P_r is the received power sensitivity, P_t is the transmitted power, and are the antenna gains of transmitter and receiver respectively. Where and denotes the power

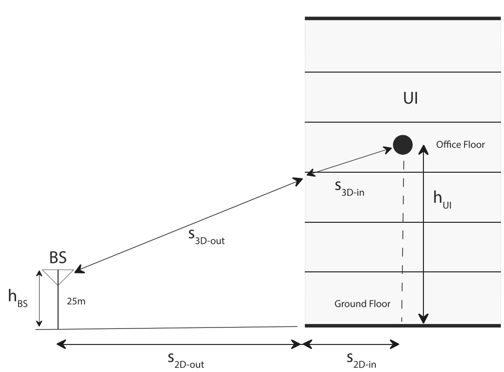

Fig. 6 Floor-wise descriptions of parameters

level and Tx-Rx separation distance accordingly. In Fig. 4a two nearest wall mounted Tx used in corridor to map the power level over random Rx positions. On the other hand, the signal penetration loss inside locations has more influence due to fluctuation of frequencies. It can be seen in Figs. 9a and 9b, which the office propagation loss is directly proportional at higher frequencies and that creates the RSS level relatively low at higher frequencies in indoor scenario.

Figures 9a and 9b illustrates that the received angular power is greater for LoS region and the received angular power for Tx simulation consequences provided in this article are in a close connection with the measurement outcomes described at reference [17]. It is experienced from the results that a sufficient indoor service can be provisioned at 28 [GHz] and 60 [GHz]. However, it is hard to provide the service to indoor mobile user at 60 [GHz] using an out-of-doors Tx even in such a small-cell environment.

4 Ray tracing concept

The idea of rays is pretty familiar to all over the experience of sun light. Rays are supposed to transmit beside a straight-line. The plane of incident is defined as the plane containing the incident, reflected and transmitted rays. In our observed case it might be a moving object (car) or static (building). As E-field is ⊥ to B-field, E-field is polarized vertically and magnetic field is polarized along horizontally. Figure 10 tells us about the free space permittivity. The dielectric constant depends upon the material on which the ray strikes. And is the standard deviation of electric field. Consider a specific ray from Omni transmitter which collide with obstacle the EM-field exerts force along horizontal i.e X-axis. The RT concept is used in mobile propagation projection more sensibly using Maxwell's and Snell's law. The electric field estimation can be expressed by

$$E_t = E_i + E_r \tag{15}$$

where E_t express the transmitted field, E_i incident angle and E_r material permittivity. Considering the polar

Fig. 7 CDF and Probability

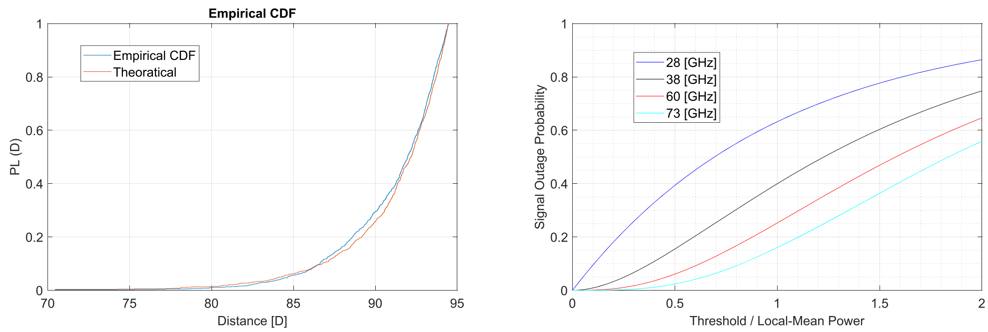

(a) (b)

Cartesian coordinate of the system, we have:

$$E_i \cos\phi_i - E_r \cos\phi_r = E_t \cos\phi_t \tag{16}$$

According to the superposition principal, the Rx detect only those rays that will have positive value of reflection coefficients. Taking into account the movement of EM-waves perpendicular as well as the parallel directions with respect to field, the coefficient of reflection become where signifies angles between the "incident rays" and the "reflected planes" and is the material permittivity of the reflected plane.

$$\Gamma_{\parallel} = \frac{E_r}{E_i} = \frac{E_i \cos\phi - \sqrt{\eta^2 - \sin^2\phi}}{E_i \cos\Phi + \sqrt{\eta^2 - \sin^2\phi}} \tag{17}$$

$$\Gamma_{\perp} = \frac{E_r}{E_i} = \frac{E_i \cos\phi - \sqrt{\eta^2 + \sin^2\phi}}{E_i \cos\Phi + \sqrt{\eta^2 + \sin^2\phi}} \tag{18}$$

In (17) and (18), ϕ is the penetrated phase angle for reflected rays and Φ is the angle for incident rays.

5 Proposed cognitive 3D RT method for UMa and indoor SBS

Cognitive Smart 3D RT is a method to find the path of each ray accurately, by recognizing and regenerating the usable paths considering the sun light theory but in the inverse order, from the receiver back to its transmitted point. Each generated ray contains some straight-lines, which are the cause of reflection, deflection and transmitted paths etc. For the reason of sorting the Tx direction of a throwing ray, the angle on the parallel surface, intended from a reference path, is called the parallel angle. Likewise, the azimuths angle on a perpendicular surface, intended from a reference path, is called the perpendicular angle. The 3D geometrical drawing of the building and floor plan is all thorough considered using MATLAB Simulink. Which consists on the structural information including concrete block walls, windows, glass type, ceilings, vehicles, tops, grid and floors. To compute and identification the path of rays, electromagnetic high-low effects on walls and on other materials are also inquired in this model as shown in Table 4. The database contain the information of concerned buildings location and distance between Tx and Rx classified in Table 4. Furthermore, based on the measurement campaign we have designed an exhaustive 3D RT propagation algorithm on 60 [GHz] mm-Wave, which uses computer-generated reality based rays and reality based simulations. It can receive the maximum transmitted propagation paths including reflected and diffracted rays regardless of any particular geometry. This smart algorithm is also autonomous in sense of treating the edges equally, either ground reflected or random diffracted. Figure 10 explains the concept of rays originating from a source and dispersing in different directions.

The behavior of algorithm comprises on two major phases Firstly find all possible sequences paths of outdoor

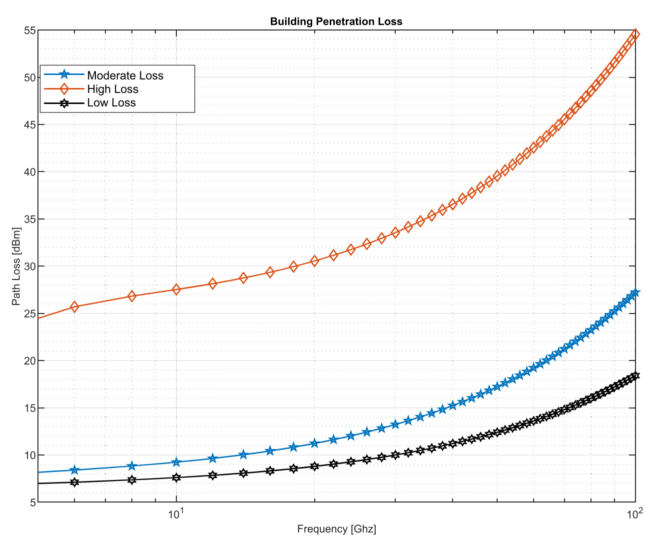

Fig. 8 High, Moderate and Low Level path loss through building external wall

and indoor, threw in various directions (horizontally or vertically) and that may produce the losses. Secondly compute the reflected and diffracted edges point for RT and finally sum-up all the path losses, i.e., loss through walls, coated glass, standard glass, wood and all metals used in scenario.

Algorithm 1 Cognitive Smart 3D Ray Tracing Algorithm for O2I

```
; for wall_out = 1 : N do
    for hori = 1 : 360° do
        for vert = 1 : 360° do
            startray[i]=1
            construct-ray=i+1
            hori −− > vert
            while wall_out = intersect do
                for j = 1 : N do
                    if dfr_out = 1 then
                        ray_dfr = ray_dfr + 1
                    else
                        ray = ray_ref
                        ray_ref = ray_ref + 1
                    end
                end
                if wall_in = intersect then
                    startray[j]=1
                    construct-ray=j+1
                    hri −− > vrt
                    while wall_in = intersect do
                        for j = 1 : N do
                            if dfr_in = 1 then
                                ray_dfr =
                                ray_dfr + 1
                            else
                                ray = ray_ref
                                ray_ref =
                                ray_ref + 1
                            end
                        end
                    end
                end
            end
            end
            end
            L_P_TOT = L_P_TYP + L_P_TB + L_P_IB + Z(0, σ²_SF)
        end
    end
end
```

Algorithm 2 Cognitive Smart 3D Ray Tracing Algorithm for I2I

```
; for j = 1 : N do
    if wall_in = intersect then
        startray[j]=1
        construct-ray=j+1
        hri −− > vrt
        while wall_in = intersect do
            for j = 1 : N do
                if dfr_in = 1 then
                    ray_dfr = ray_dfr + 1
                else
                    ray = ray_ref
                    ray_ref = ray_ref + 1
                end
            end
        end
        end
        L_P_in−ofc =
        38.3log10(S_3D) + 17.20 + 24.9log10(f_c)
    end
end
```

6 Results validation and discussion

The results validation and discussions are provided here in the form of path loss over distance, received signal power level and outcomes from proposed smart 3D RT algorithm in this simulation. The simulations were done using dimension layouts of the building which were designed in the MATLAB Simulink.

6.1 Cognitive ray tracing O2I environment

Figures 14a and 14b show 2D and 3D respectively is the representation of rays transmitted from the tip of Tx on 25 [m] height and penetrated in third floor of building through number of obstacles. A smart cognitive RT algorithm is executed in MATLAB. Figure 14a illustrates the location of Rx which is inside the B2 as marked in green color. In Fig. 14b three dimensional illustration of the proposed algorithm is presented with its building set-up, where Tx is erected outside and simulated rays in red and green color compared on multiple receiving locations. It can be seen that the incident rays sometime reached via direct path and sometime finite number of reflection, transmission and diffraction occurred due to ground and building edges. Fig. 15a shows the path loss trend when Tx and Rx are

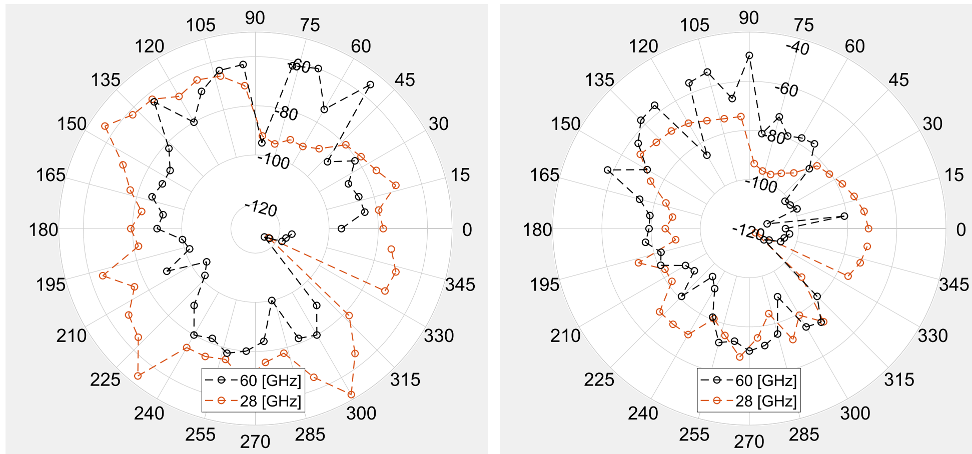

(a) (b)

Fig. 9 Received angular power at 28 [GHz] and 60 [GHz]

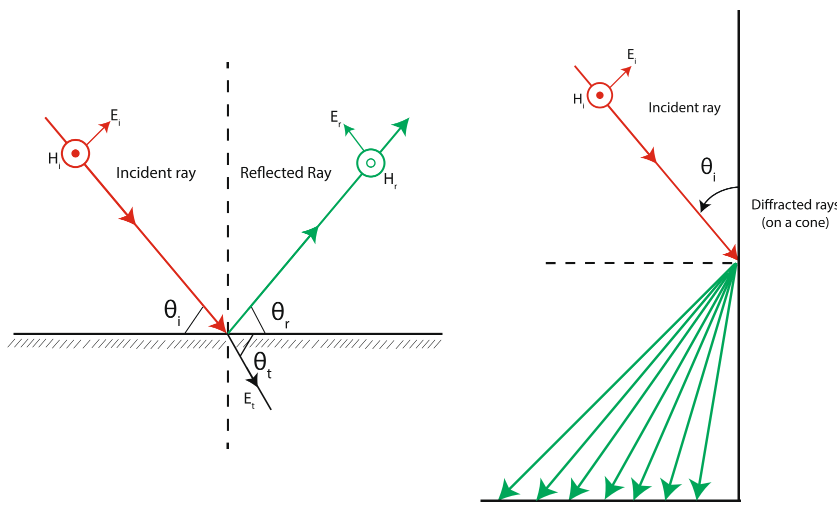

Fig. 10 Ray concept for plane and normal to plane of incidence

Table 4 High operating frequencies properties over different construction materials

PL Model	Dependency on Frequency	28 [GHz]	60 [GHz]
Low	$5 - 10log_{10}(0.7 * 10^{-\frac{L_{Con}}{10}} + 0.3 * 10^{-\frac{L_{SG}}{10}})$	9.8 [dBm]	13.6 [dBm]
Moderate	$5 - 10log_{10}(0.7 * 10^{-\frac{L_{pwd}}{10}} + 0.3 * 10^{-\frac{L_{Con}}{10}})$	13.2 [dBm]	17.3 [dBm]
High	$5 - 10log_{10}(0.7 * 10^{-\frac{L_{MCG}}{10}} + 0.3 * 10^{-\frac{L_{Con}}{10}})$	32.9 [dBm]	42.6 [dBm]

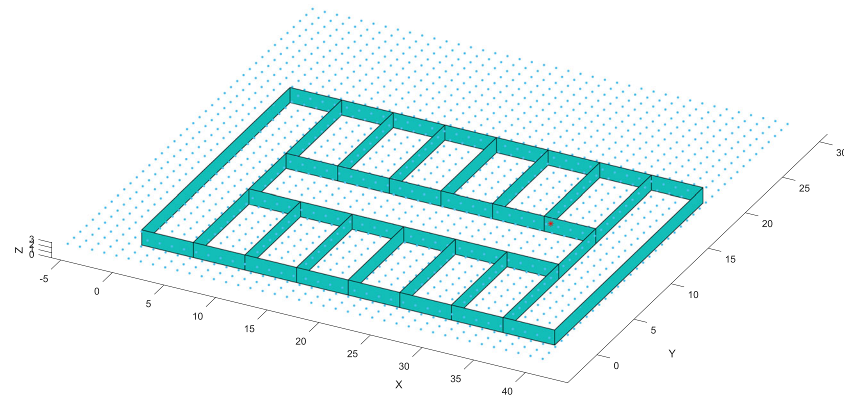

Fig. 11 Indoor 3D architecture in MATLAB

parallel to each other in term of their height, i.e., 25 [m] and their separation distance 50 [m]. We have seen that on direct path, the loss is comparatively low around 147 [dB] and presented in red color as there are less obstacles. On the other hand, Fig. 15b is the representation of high path loss 170 [dB] for 110 [m] separation distance. In 3D path loss graph, the dimmest blue square clearly indicates that the rays are received through indirect path as shown in Fig. 15. The reason behind is that the B4 is raised in the front of concerned B2 with 30 [m] height and there is no direct path on receiving end. So it can be seen the path loss is radically increased from 4th floor to ground floor as rays received through scatters. Moreover, when concerned frequency compared with 28 [GHz] operating frequency, it has been noticed that the Path Loss Exponent (PLE) also increased due to the small wave length and variation in between Tx and Rx distance. Figures 14 and 15 also shows the impact of signal strength over distance, where on the right side of graph the scale presented the path loss in dB which is directly propositional to the distance as well as

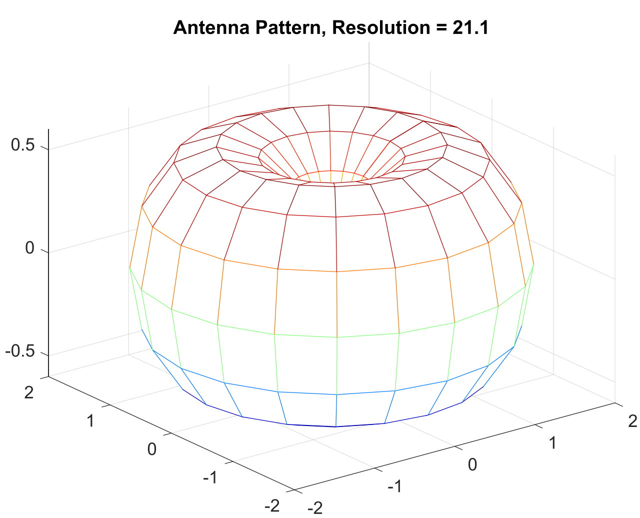

Fig. 12 Antenna Pattern for Omni-Directional at 60 [GHz]

received power. For simulating the rays in smart algorithm, the B1 and B3 edges are work as perfect mirror, in which the angle of incidence is parallel to the angle of reflection and transmitted rays are discarded during computation. The receivers are pointing on multiple floors in B2, so in this case the incidence ray first penetrate into ceilings and then finally reach to receiver. To compute the losses of plywood, ceilings, standard glass, metal coated glass and concrete, we have added the penetration models for all related hindrances in this work. Normally, the ceilings are made with concrete, so in this work the concrete penetration parameters are similar for ceilings loss.

6.2 Smart ray tracing for indoor corridor and open office

Figure 8 shows through wall penetration loss for a range of frequencies. The variation in loss models is due to the material used in buildings and small wave length of higher radio channels. Figure 11 shows the indoor 3D architecture (floor wise) with corridor length and open office partitions on different receiving points, which is planned in MATLAB. The reflectivity of the partitions and the edges of the partitions can be found out by detecting the path of rays. Figure 12 shows the antenna pattern for Omni-Directional, its beam-width (degree), height [m] and radio frequency (GHz) values are given in Table 3 parameter set-up.

Figure 13 explains the open office and corridor received power (Tx-Rx) simulation and significance provided in this article have close connection with the measurement outcomes described at reference [17]. It is experienced from the results that a sufficient indoor service can be provisioned at 28 [GHz] and 60 [GHz]. However, it is bit hard to provide the services to indoor users at 60 [GHz] using an out-of-doors Tx, even in a small cell environment. Figure 13 is the graphical representation of path loss from corridor to open office. The heat-maps show power radiated by transmitter at different locations. The yellow color in the graph shows the reception sensitivity which becomes darker when receiver

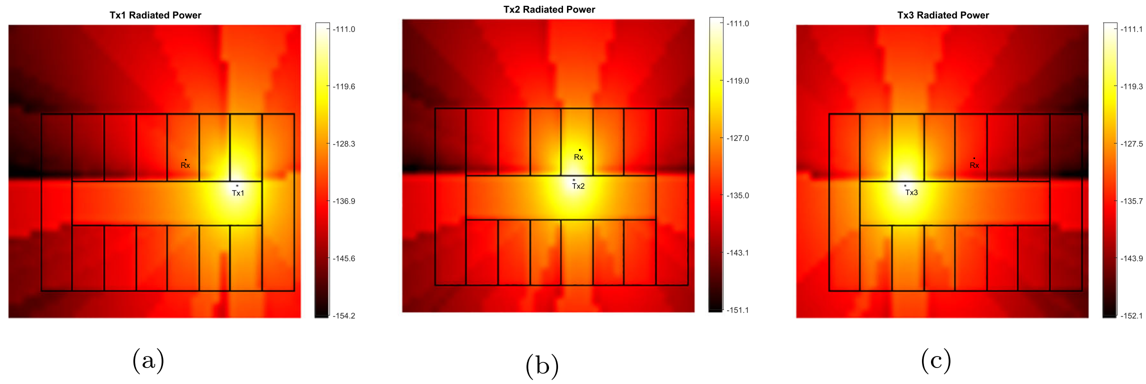

Fig. 13 Radiated power for different locations of Tx

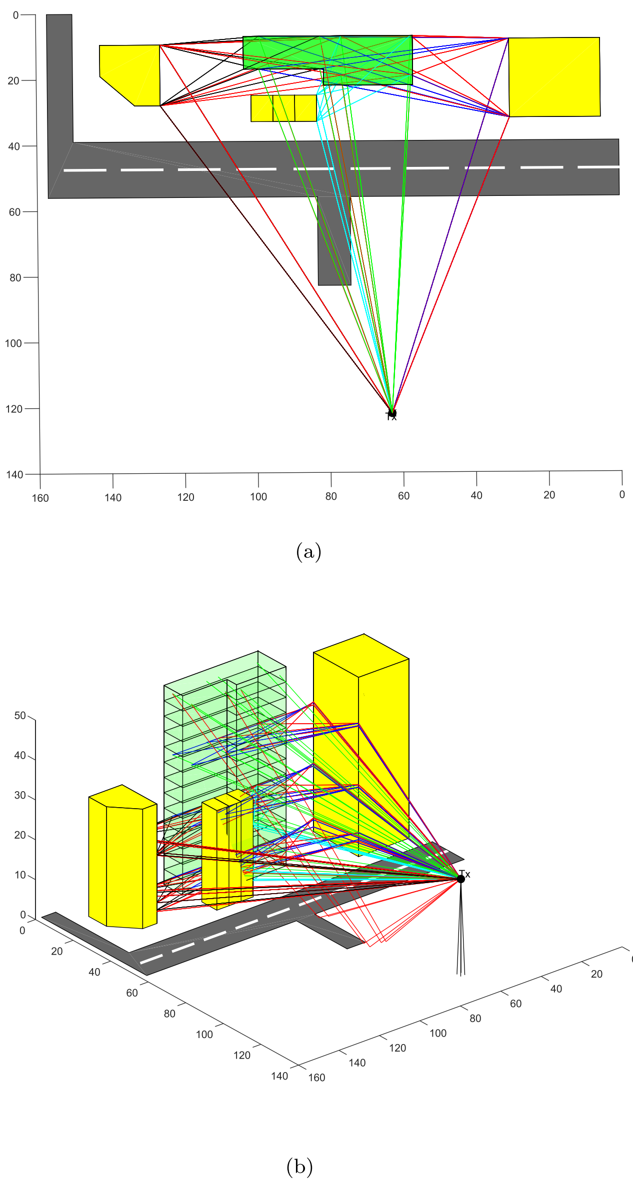

Fig. 14 2D and 3D representation of transmitted rays

gets far away from the radiated point, where the highest signal throughput is -120 dBm approx in (Fig. 13b) $Tx2$ location. The weak signal strength is noticeable from the walls in 1st reflection which is affected by reflection and diffraction. Furthermore, Fig. 13 shows the received power -113 dBm for LoS at perpendicular angle (azimuth plane). Altogether, we improved ray pointing technique to make the proposed 3D ray tracing algorithm more efficient, suitable and smart. From the results and considerations, it is clear that the suggested ray tracing method has significant impact on mobile radio propagation in term of large scale path loss, received angular power and number of received rays. The results also explained here that (Figs. 14 and 15)

- For LoS on 60 [GHz] the RSS is -40 dBm on 90° angle and compare to 28 [GHz] the RSS is -75 dBm. Secondly, for NLoS on same angle and frequencies the RSS value is -95 dBm and -80 dBm respectively. So above mentioned ideals values also shows great agreement with literature [5], where it can be seen clearly that received angular power is improved individually -35 dBm and -15 dBm on high operating frequency.
- Distance is directly proportional to pathloss. The heapmap tells us that the increasing the distances and number of hurdles could result in greater pathloss.

7 Conclusions

In this article, we presented a smart 3D ray tracing algorithm to examine outdoor and indoor radio propagation at 60 [GHz] and results also compared with our previous work. The algorithm pointing more rays only in the predefined region, which improve the computational efficiency in densely populated area. With the help of real time capabilities, geospatial awarnesses, the path loss, signal

Fig. 15 Heapmaps for different Tx-Rx separations

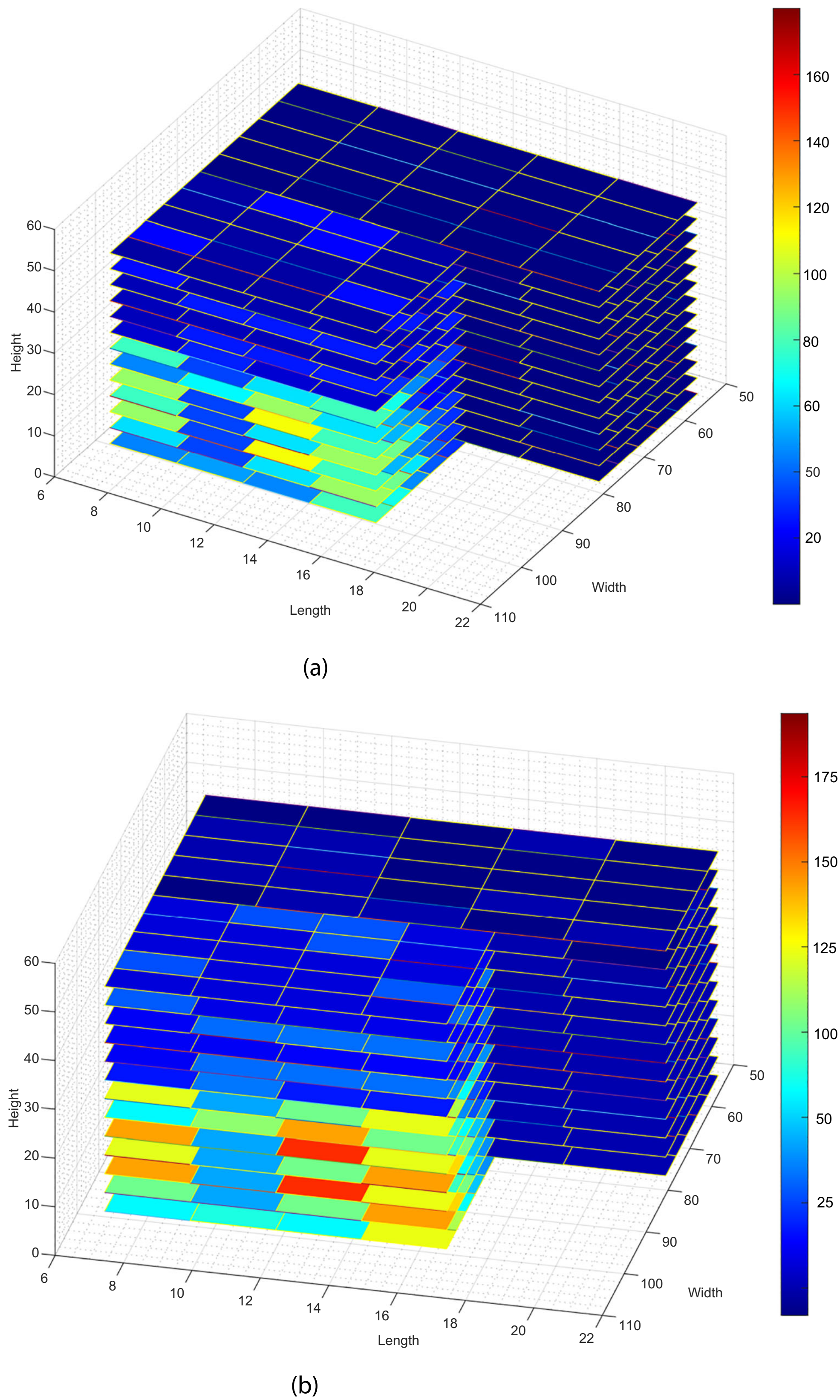

strength and propagation delays can be determined in cognitive radio networks. [19].

The path loss and reception sensitivity were validated by the use of the recent 3GPP mobile propagation model. The article findings suggest that the millimeter wave's propagation heavily attenuates with the increasing separation between the transmitter and the receiver. Besides this, the obstacles and hurdles in the path of waves can cause reflection and diffractions which can result in large path loss and low received signal strength. The Simulator used in this article is designed in MATLAB. This can be used for any site regardless of the geometry of the buildings and environment chosen. By changing the antenna parameters, physical layout of the building, material used in building (glass, concrete), operating frequency), location of Tx-Rx and separation between Tx-Rx, this simulator can be used for any environment. The results gap show that the proposed ray tracing is more perfect with respect to RSS and path loss. The contributions of this study is expected to guide further research on 60 [GHz] and 73 [GHz] mmWave particularly in-building environment.

References

1. Ullah U, Kamboh UR, Hossain F, Danish M (2020) Outdoor-to-indoor and indoor-to-indoor propagation path loss modeling using smart 3D ray tracing algorithm at 28 GHz mmWave. Arab J Sci Eng, pp 1–10
2. Shah SA, Fan D, Ren A et al (2020) Seizure episodes detection via smart medical sensing system. J Ambient Intell Human Comput 11:4363–4375. https://doi.org/10.1007/s12652-018-1142-3
3. Suleyman N (2020) Comparision of field measurement data with propagation models, and modification of COST 231-Hata and Cost 231-Walfisch-Ikegami propagation models for UMTS2100 mobile network in Ashgabat, Koshi. In: Digitalization and Industry 4.0: Economic and Societal Development (pp. 105–118). Springer Gabler, Wiesbaden
4. Rappaport TS, Heath RW, Daniels Jr. RC, Murdock JN (2015) Millimeter wave wireless communications. Englewood-Cliffs, NJ, USA: Prentice-Hall
5. Al-Turjman F (2019) 5G-enabled devices and smart-spaces in social-IoT: An overview. Future Generation Computer Systems 92:732–744. ISSN 0167-739X, https://doi.org/10.1016/j.future.2017.11.035
6. Maltsev A, Maslennikov R, Sevastyanov A, Khoryaev A, Lomayev A (2009) Experimental investigations of 60 GHz WLAN systems in office environment. IEEE J Sel Areas Commun 27(8):1488–1499
7. Amjad K, Ali M, Jabbar S, Hussain M, Rho S, Kim M (2015) Impact of dynamic path loss models in an urban obstacle aware ad hoc network environment. Journal of Sensors 2015:8. https://doi.org/10.1155/2015/286270. Article ID 286270
8. Shah SA et al (2017) Buried object sensing considering curved pipeline. In: IEEE antennas and wireless propagation letters, vol 16, pp 2771–2775. https://doi.org/10.1109/LAWP.2017.2745501
9. Fu W, Hu J, Zhang S (2013) Frequency-domain measurement of 60 GHz indoor channels: A measurement setup, literature data, and analysis. IEEE Instrum Meas Mag 16(2):34–40
10. Haneda K, Karttunen A, Kyrö M, Putkonen J (2014) Indoor short-range radio propagation measurements at 60 and 70 GHz. In: Proc. 8th Eur. Conf. Antennas Propag. (EuCAP), pp 634–638
11. Gutiérrez O, Adana FS, González I, Pérez J, Cátedra MF (2000) Ray-tracing techniques for mobile communications. ACES J 15(3):209–231
12. McNamara DA, Pistorius CWI, Malherbe LAG (1990) Introduction to the uniform geometrical theory of diffraction. Norwood MA: Artech house
13. Kiran J, Nimavat D (2015) Comparative analysis of path loss propagation models in radio communication. In: IJIRCCE, vol. 3, no. 2
14. Geok TK, Hossain F, Kamaruddin MN, Rahman NZA, Thiagarajah S, Chiat ATW, Liew CPA (2018) Comprehensive review of efficient ray-tracing techniques for wireless communication. International Journal on Communications Antenna and Propagation 8(2):123–136
15. Shabbir G, Akram A, Munwar Iqbal M, Jabbar S, Alfawair M, Chaudhry J (2020) Network performance enhancement of multi-sink enabled low power lossy networks in SDN based internet of things. International journal of parallel programming Springer 48(5):367–398
16. Yue G, Yu D, Qiu H, Guan K, Yang L, Lv Q (2019) Measurements and ray tracing simulations for non-line-of-sight millimeter-wave channels in a confined corridor environment. IEEE Access 7:85066–85081
17. Tateishi K et al (2015) Field experiments on 5G radio access using 15-GHz band in outdoor small cell environment, Personal, Indoor and Mobile Radio Communications (PIMRC), 2015 IEEE 26th Annual International Symposium on Hong Kong, pp 851–855
18. Hossain F, Geok TK, Rahman TA, Hindia MN, Dimyati K, Ahmed S, Tso CP, Abd Rahman NZ (2019) An Efficient 3-D Ray Tracing Method: Prediction of Indoor Radio Propagation at 28 GHz in 5G Network. Electronics 8:286
19. Roy A, Sengupta S, Wong K-K, Raychoudhury V, Govindan K, Singh S (2017) 5G Wireless with Cognitive Radio and Massive IoT, IETE Technical Review, 34:sup1, 1–3. https://doi.org/10.1080/02564602.2017.1414387
20. Vitucci EM, Degli-Esposti V, Fuschini F, Lu JS, Barbiroli M, Wu JN, Zoli M, Zhu JJ, Bertoni HL, Ray Tracing RF (2015) Field Prediction: An Unforgiving Validation, International Journal of Antennas and Propagation, vol. 2015, Article ID 184608 11 pages. https://doi.org/10.1155/2015/184608
21. Zöchmann E, Guan K, Rupp M (2017) Two-ray models in mmwave communications. In: Proc IEEE Int Workshop Signal Process. Advances Wireless Commun. (SPAWC), Sapporo, pp 1–5, Japan
22. He R, Zhong Z, Ai B, Ding J, Guan K (2012) Analysis of the relation between fresnel zone and path loss exponent based on two-ray model. IEEE Antennas Wireless Propag Lett 11:208–211
23. Wang Y, Zhang N, Zhang Q, Ye J (2007) A 2-Ray path loss model for i-UWB signals transmission. In: Proc Int Conf Wireless Commun Netw Mobile Comput, pp 554–556, Shanghai, China
24. Supanakoon P, Chaiyapong S, Promwong S, Takada J (2011) Threeray path loss based on peak power loss for ultra wideband impulse radio systems. In: Proc Int Symp Intell Signal Process Commun Syst (ISPACS), pp 1–4, Chiang Mai, Thailand

25. Faruque S (1995) A three ray propagation model for PCS and micro-cellular services. In: Proc IEEE Military Commun Conf (MILCOM), vol. 3, pp 1239–1243. San Diego, CA, USA
26. Han C, Bicen AO, Akyildiz IF (2015) Multi-ray channel modeling and wideband characterization for wireless communications in the terahertz band. IEEE Trans Wireless Commun 14(5):2402–2412
27. Oo K, Aye A (2018) Analysing of indoor LOS radio wave propagation model using ray tracing technique. Int J Sci Eng Technol Research 7:623–628
28. Rapaport L, Etinger A, Litvak B, Pinhasi G, Pinhasi Y (2018) Quasi optical multi-ray model for wireless communication link in millimeter wavelengths. In: Proc. MATEC Web Conf, vol. 210, pp 03006. EDP Sciences
29. Etinger A, Litvak B, Pinhasi Y (2017) Multi ray model for near-ground millimeter wave radar. Sensors 17(9):1983
30. Bhuvaneshwari A, Hemalatha R, Satyasavithri T (2015) Path loss prediction analysis by ray tracing approach for NLOS indoor propagation. In: Proc. IEEE Int. Conf. Signal Process. Commun. Eng. Syst., Guntur, India
31. Khawaja W, Ozdemir O, Erden F, Ozturk E, Guvenc I (2020) Multiple ray received power modeling for mmWave indoor and outdoor scenarios. arXiv: Signal Processing
32. Hossain F, Geok T, Rahman T, Hindia M, Dimyati K, Ahmed S, Tso C, Rahman A, Ziela N (2019) An efficient 3-D ray tracing method: Prediction of indoor radio propagation at 28 GHz in 5G network. PLoS ONE. 8. 286. https://doi.org/10.3390/electronics8030286
33. Marai M, Ismail M, Misran N (2011) Validation of three-dimensional ray-tracing algorithm for indoor wireless propagations. ISRN Communications and Networking. 2011. https://doi.org/10.5402/2011/324758
34. Wu C-Y, Yen H-S, Chiu C-C, Chiang J-S, Chang C-W (2014) Urban area propagation path loss reduction by dynamic differential evolution algorithm. 2014, International conference on intelligent green building and smart grid (IGBSG). https://doi.org/10.1109/igbsg.2014.6835257
35. Al-Turjman F, Ever E, Zahmatkesh H (2018) Small cells in the forthcoming 5G/IoT: Traffic modelling and deployment overview. IEEE Communications Surveys & Tutorials, pp 1–1. https://doi.org/10.1109/comst.2018.2864779

Publisher's note Springer Nature remains neutral with regard to jurisdictional claims in published maps and institutional affiliations.

Usman Rauf Kamboh was born in Gujranwala, Punjab Province, Pakistan, in 1987. He obtained his M.Sc. degree in Computer Networks from University of the Punjab in 2010, and the Ph.D. degree in Information & Communication System from Xidian University, Xi'an, China, in July 2018. He started his Ph.D. curriculum in October 2015 in the Department of Communication and Computer computer networks. From 2014 to 2018 he has been awarded a scholarship under the China Scholarship Council (CSC) to pursue his research in People's Republic of China as a joint Ph.D. student between School of International Education (SIE) and The State Key Laboratory of ISN Xi'an, China. He has also held appointments as visiting scholar at number of universities in Pakistan and China. His is serving as an assistant professor at The University of Faisalabad at the department of computer sciences since august, 2018. His research field is mainly about Techno-Economics and management of cellular networks, pathloss, UAVs artificial neural networks, artificial intelligence and millimeter wave and mmWave.

Mr. Ubaid Ullah received his B.S. degree in Computer System from COMSATS Institute of Information Technology, Islamabad, in the year 2011. In 2014 he received his MS(Telecommunication with specialization in computer networks) from the University of Sunderland, UK. In 2014, he joined department of Electrical Engineering at Federal Urdu University as a visiting Lecturer. He joined TUF in 2016 as a permanent faculty member and in been serving The University of Faisalabad since 2016. His research interests include radio waves path loss artificial neural networks, artificial intelligence and millimeter wave and link budget management.

Dr. Shehzad Khalid is working as a professor at the Department of Computer Engineering, Bahria University Islamabad. He is currently designated as a Director (ORIC) in Head office of Bahria University. He is completed his Bachelor of Science in Computer Systems Engineering from GIK Institute of Engineering Sciences & Technology Topi, in 2000. He has received her master?s degree in MSc Software Engineering from National University of Science and Technology, Rawalpindi, in 2003. And awarded to Ph.D. degree in Motion Data Mining and Machine Learning, February, from University of Manchester, UK. in 2009. His research areas are Computer Vision and Pattern Recognition. He is also headed by research group "Computer Vision and Pattern Recognition Research Center". He has completed his 76 publications so far including 8 ISI indexed and 68 journal papers and 43 conference papers. He has completed 9 research project and published 5 book chapters and 1 complete book. He is received 18 different awards which is including Best researcher and Best Teacher from Bahria University and Higher Education Commission Pakistan and other organizations. He is supervised 17 MS Students and 8 PhD students.

Dr. Umar Raza is a Lecturer at Manchester Metropolitan University in Computer and Network technology. He received his PhD in Service Orientated Architecture (SOA) and Wireless Sensor Networks (WSN) approach applied to the measurement and visualisation of a μInjection Molding Process from the University of Bradford Polymer IRC Laboratory. His previous experience includes seven years in the industry as a Software Engineer and over eight years of experience as a Lecturer in Robotics, Networking, and Computing at Staffordshire University. His current research interests and expertise include track and trace of pharmaceutical drugs using RFID and Blockchain technology, Industrial IoT data analytics and security, attribute-based authentication for IoT devices, data semantics and ontologies for Cyber-Physical systems. Application of machine learning in security, industrial, and assisted living fields using IoT devices.

Chinmay Chakraborty is an Assistant Professor (Sr.) in the Dept. of Electronics and Communication Engineering, Birla Institute of Technology, Mesra, India. His primary areas of research include Wireless Body Area Network, Internet of Medical Things, and Telemedicine. He worked at the Faculty of Science and Technology, ICFAI University, Agartala, Tripura, India as a Sr. lecturer. He worked as a Research Consultant in the Coal India project at Industrial Engineering & Management, IIT Kharagpur. He worked as a project coordinator of Telecom Convergence Switch project under the Indo-US joint initiative. He also worked as a Network Engineer in System Administration at MISPL, India. He has authored or co-authored over 60 publications in refereed international journals, conferences, book chapters, and books. He is an Editorial Board Member in the different Journals and Conferences. He is a guest editor of Future Internet journal special issue and SoCTA-19 International Conference. Dr. Chakraborty is a member of Internet Society, Machine Intelligence Research Labs, and Institute for Engineering Research and Publication. He received young research excellence award, Global Peer Review Award, Young Faculty Award and Outstanding Researcher Award.

Prof. Dr. Fadi Al-Turjman received his Ph.D. in computer science from Queen?s University, Kingston, Ontario, Canada, in 2011. He is a full professor and a research center director at Near East University, Nicosia, Cyprus. Prof. Al-Turjman is a leading authority in the areas of smart/intelligent, wireless, and mobile networks? architectures, protocols, deployments, and performance evaluation. His publication history spans over 250 publications in journals, conferences, patents, books, and book chapters, in addition to numerous keynotes and plenary talks at flagship venues. He has authored and edited more than 25 books about cognition, security, and wireless sensor networks? deployments in smart environments, published by Taylor and Francis, Elsevier, and Springer. He has received several recognitions and best papers? awards at top international conferences. He also received the prestigious Best Research Paper Award from Elsevier Computer Communications Journal for the period 2015-2018, in addition to the Top Researcher Award for 2018 at Antalya Bilim University, Turkey. Prof. Al-Turjman has led a number of international symposia and workshops in flagship communication society conferences. Currently, he serves as an associate editor and the lead guest/associate editor for several well reputed journals, including the IEEE Communications Surveys and Tutorials (IF 23.9) and the Elsevier Sustainable Cities and Society (IF 5.7).

Affiliations

Usman Rauf Kamboh[1] · **Ubaid Ullah**[1] · **Shehzad Khalid**[2] · **Umar Raza**[3] · **Chinmay Chakraborty**[4] · **Fadi Al-Turjman**[5]

Ubaid Ullah
ubaid.ullah@tuf.edu.pk

Shehzad Khalid
shehzad_khalid@hotmail.com

Umar Raza
u.raza@mmu.ac.uk

Chinmay Chakraborty
cchakrabarty@bitmesra.ac.in

Fadi Al-Turjman
fadi.alturjman@neu.edu.tr

1 Department of Computational Sciences, The University of Faisalabad, Faisalabad, Pakistan

2 Department of Computer Engineering, Bahria University, Islamabad, Pakistan

3 Department of Engineering, Manchester Metropolitan University, Manchester, England

4 Dept. of Electronics & Communication Engineering, Birla Institute of Technology, Jharkhand, India

5 Research Center for AI and IoT, Near East University, Nicosia, Mersin 10, Turkey